On the Characterization of Host–Guest Complexes: Surface Tension, Calorimetry, and Molecular Dynamics of Cyclodextrins with a Non-ionic Surfactant

**Ángel Piñeiro,*,† Xavier Banquy,† Silvia Pérez-Casas,† Edgar Tovar,† Abel García,†
Alessandra Villa,‡ Alfredo Amigo,§ Alan E. Mark,‖,⊥ and Miguel Costas*,†**

*Laboratorio de Biofisicoquímica, Departamento de Fisicoquímica, Facultad de Química, Universidad Nacional
Autónoma de México, Cd. Universitaria, México D.F. 04510, Mexico, Institute for Physical and Theoretical
Chemistry, J.W. Goethe University, Max-von-Laue 7, 60439 Frankfurt, Germany, Departamento de Física
Aplicada, Facultad de Física, Universidad de Santiago de Compostela, E-15782, Santiago de Compostela,
Spain, Groningen Biomolecular Sciences and Biotechnology Institute (GBB), Department of Biophysical
Chemistry, University of Groningen, Nijenborgh 4, 9747 AG Groningen, The Netherlands, and School of
Molecular and Microbial Sciences and the Institute for Molecular Biosciences, University of Queensland,
Saint Lucia, 4072, Queensland, Australia*

Three host–guest systems have been characterized using surface tension (σ), calorimetry, and molecular dynamics simulations (MD). The hosts were three native cyclodextrins (CD) and the guest the non-ionic carbohydrate surfactant octyl-β-D-glucopyranoside. It is shown that, for any host–guest system, a rough screening of the most probable complex stoichiometries can be obtained in a model free form, using only calorimetric data. The σ data were analyzed using a model that includes a newly proposed adsorption isotherm. The equilibrium constants for several stoichiometries were simultaneously obtained through fitting the σ data. For α- and β-CD, the predominant species is 1:1 and to a lesser extent 2:1, disregarding the existence of the 1:2. For γ-CD, the 1:2 species dominates, the other two being also present. In an attempt to confirm these results, 10 ns MD simulations for each CD were performed using seven different starting conformations. The MD stable conformations agree with the results found from the experimental data. In one case, the spontaneous dissociation–formation of a complex was observed. Analysis of the trajectories indicates that hydrophobic interactions are primarily responsible for the formation and stability of the inclusion complexes. For the 2:1 species, intermolecular H-bonds between CD molecules result in a tight packed structure where their original truncated cone shape is lost in favor of a cylindrical geometry. Together, the results clearly demonstrate that the often used assumption of considering only a 1:1 species is inappropriate.

1. Introduction

A detailed understanding of the factors that determine the formation and properties of molecular assemblies such as host–guest complexes, cyclodextrin necklaces, ligand–protein complexes, and protein–protein complexes is not only of fundamental scientific interest but also a prerequisite for the development of technologies in areas ranging from molecular machines to structure-based drug design.[1–10] Comprehension of the molecular recognition process requires both knowledge of the thermodynamic properties of the system and an insight into the structure and dynamics of the molecular assembly. A combination of these two levels of description allows a more complete characterization of the systems under examination. In this work, macroscopic thermodynamic measurements are combined with atomistic molecular dynamics simulations to study a particular subset of molecular assemblies, namely a series of inclusion complexes.

At the thermodynamic or macroscopic level, the stability of molecular assemblies with the general formula A_nB_m is fre-

quently characterized by the change in Gibbs energy ΔG or the equilibrium constant K for the formation of each species. The determination of the number of different species in equilibrium, and their stoichiometries, is a crucial first step toward the characterization of the system. In principle, the equilibrium constants can be obtained by directly measuring the concentration of the free components (A and B) and each complex species (A_nB_m) in the mixture. For the majority of the systems, this is a difficult if not impossible task. Instead, equilibrium constants are obtained through the application of models, where the several K are fitting parameters, to some experimentally measured quantity. The model that best fits the data is then assumed to reflect the nature of the species in solution. To this end, isothermal titration calorimetry, capillary electrophoresis, NMR, and affinity chromatography[11–15] are some of the most frequently employed experimental techniques. This approach has two difficulties. First, a given experimentally determined property may not be sufficiently sensible to elucidate the presence of multiple species A_nB_m. This can easily be the case even if the property is measured as a function of more than one variable, typically concentration and temperature. For this reason, when trying to characterize molecular assemblies, it is highly recommended to employ more than one property. Second, the level of complexity of the models developed to describe the data increases with the number of species consid-

* E-mail: fangel@servidor.unam.mx (Á.P.); costasmi@servidor.unam.mx
(M.C.).
† Universidad Nacional Autónoma de México.
‡ J.W. Goethe University.
§ Universidad de Santiago de Compostela.
‖ University of Groningen.
⊥ University of Queensland.

ered to be present in the system. As more complex A_nB_m stoichiometries are taken into account, the larger the number of adjustable parameters and the greater their statistical uncertainty upon fitting. As a result, in many instances, model fitting cannot be used to discern if more than one A_nB_m species is present. To overcome both difficulties, an often used simplifying assumption is to consider that only the simplest stoichiometry, i.e., the 1:1 complex species (A_1B_1), is present.[11,16-19] In this work, we propose a straightforward test of this assumption that relies only on experimental calorimetric data and provides a rough qualitative screening of the species in solution. To obtain a quantitative characterization of the host−guest complexes under study, we have elected to employ liquid−vapor surface tension (σ) measurements. Two factors directed this election, namely that σ is very sensitive to the concentration of the different species in the bulk liquid and that it can be determined with a high level of accuracy. To analyze the σ data, a model that combines a newly proposed adsorption isotherm with a mixing rule was developed. In this model, the equilibrium constants for a number of stoichiometries are simultaneously obtained, providing the relative population of each species and indicating those whose concentration is negligible. These equilibrium constants, in turn, were used to obtain the enthalpies for complex formation from isothermal titration microcalorimetry data. We demonstrate that this approach is a suitable strategy to achieve a thermodynamic description of molecular assemblies with multiple stoichiometries.

In an attempt to confirm the stability of the specific species suggested by the thermodynamic analysis, a series of atomistic MD simulations were also performed. Although this technique has been used successfully to study many inter- and intramolecular assemblies,[20-23] few MD studies[24] have been directed toward the elucidation of both the structure and stoichiometry of the simulated complexes, i.e., simulations where the starting configuration is not known from either X-ray crystallography or NMR or has been computationally docked. The MD simulations were performed starting from prearranged configurations for the most likely inclusion complex stoichiometries and relative orientations between molecules. Notably, the results from the MD simulations indicate that the most probable stoichiometries are precisely those suggested by the thermodynamic analysis of the system. Furthermore, the simulations provide microscopic insight into the main factors that determine the stability of the host−guest complexes.

The molecular assemblies considered in this work to test the proposed methodology were inclusion complexes formed by a non-ionic carbohydrate surfactant (octyl-β-D-glucopyranoside or OGP) and three native α-, β-, and γ-cyclodextrins (CD) in aqueous solution. These systems were selected for several reasons, the most important being the high probability that different stoichiometries coexist in equilibrium, the high critical micelle concentration of OGP that facilitates the experiments, and the absence of ionic species in solution that simplifies the application of thermodynamic models as well as the MD simulations.

2. Experimental Methods

2.1. Materials. Octyl-β-D-glucopyranoside (OGP) was obtained from Aldrich with a stated purity of $\geq$98%. The cyclodextrins (CD) were a generous gift from Cerestar (Cargill Co., U.S.A.) with a purity of >99% for α- and γ-cyclodextrins and >98% for β-cyclodextrin. Their water content was determined by Karl Fischer titration (701 KF Titrino, Metrohm, Switzerland). All chemicals were used without further purifica-

tion. Water was distilled and deionized using Barnstead Nanopure Infinity equipment, its resistivity being 18.0 ± 0.2 MΩ cm^{-1}. Prior to use, water was degassed. The solutions were carefully prepared by mass (model AT250, Mettler, Switzerland) taking into account the water content of each CD.

2.2. Surface Tension. For each cyclodextrin, liquid−vapor surface tensions (σ) at 298.15 ± 0.01 K were determined for four series of mixtures. Solutions in each of these series contained a fixed concentration of CD (ranging from 1 to 30 mM) and increasing amounts of OGP. The OGP concentration varied from zero to a value slightly above its apparent critical micelle concentration (cmc$_{ap}$) at that particular CD concentration. Surface tensions were determined using a Lauda drop volume tensiometer (TVT-1 model, Lauda, Germany) previously described in detail.[25] To avoid hydrodynamic effects, the standard mode where the plunger velocity is reduced four times during the creation of each drop was employed. The optimum initial dropping time was 0.15 s μL^{-1}. Solutions were injected from a 2.5 mL syringe through a capillary of inner radius 1.70 mm. To guarantee equilibrium between the sample liquid in the drops and the surrounding vapor space where they form, a small sample of the solution in the syringe was placed in the closed vessel where the drops fall down. The syringe and vessel temperature was controlled within 0.01 K using a thermostat (model F10&MH, Julabo, Germany). Through repetition of the present measurements, the accuracy of the surface tensions appears to be 0.02 mN m^{-1}.

2.3. Calorimetry. The calorimetric measurements were performed at 298.15 ± 0.01 K using a Thermal Activity Monitor (TAM) model 2277 from Thermometric (Sweden) equipped with a 2201 high performance calorimetric unit. Under optimal conditions, this instrument is capable of detecting ± 1 μWatt. Approximately 2 mL of an aqueous solution of cyclodextrin was introduced into the sample and reference cells, each with a total volume of 4 mL. A solution of OGP between 218 and 222 mM, approximately 10× its cmc, was titrated to the sample cell employing a syringe pump model 612 Lund from Thermometric (Sweden) controlled by a computer. In all experiments, 10 μL titrations were used. At the end of the experiment, the OGP concentration in the sample cell was higher than its cmc$_{ap}$ at that particular CD concentration. Pure water was simultaneously titrated into the reference cell to subtract from the total signal the heat due to the dilution of the cyclodextrin. For each of the three cyclodextrins, experiments using the above-described methodology were performed at several CD concentrations, ranging from 7 to 17 mM. The OGP dilution experiment, where OGP at a concentration approximately 10× its cmc was titrated into pure water, was also performed. At the start and end of each experiment, an electric calibration of the calorimetric unit was carried out in order to adjust the power sensor in the cells.

2.4. MD Simulations. The MD simulations were performed using the GROMACS package[26-28] (version 3.2.1) with the simple point charge (SPC) water model[29] and with a modified version of the GROMOS96 (45a3) force field[30] with the parameters for oligosacharides and hydrophobic interactions as later incorporated in the 53a6 force field.[31] This force field treats each aliphatic carbon atoms together with their attached hydrogen atoms as a single unit. Periodic boundary conditions, with a rhombic dodecahedron box as the basic unit cell in the *NPT* ensemble, were used. The size of the boxes was chosen with a distance of 5 nm between the centers of two contiguous images, in order to prevent direct interactions between periodic images of the same molecule. Boxes were filled with between

Characterization of Host−Guest Complexes

J. Phys. Chem. B, Vol. 111, No. 17, 2007 **4385**

2700 and 2900 pre-equilibrated water molecules and the system energy minimized. The pressure was maintained by weak coupling to 1 bar by means of a Berendsen barostat,[32] with a coupling time of 0.5 ps and an isothermal compressibility of 4.6×10^{-5} bar^{-1}. The initial coordinates of the cyclodextrins and OGP atoms were taken from the Brookhaven Protein Data Bank (PDB structures 1BTC, 3CGT, 1D3C, and 2IWW). For each of the three cyclodextrins, seven different starting conformations for the CD/OGP complexes were constructed. These 21 initial structures correspond to all of the possible relative orientations that the CD and OGP molecules can adopt in the 1:2 and 2:1 stoichiometries. Water, cyclodextrin, and OGP molecules were coupled separately to a temperature bath at 298 K (using a coupling constant of 0.1 ps) by means of a Berendsen thermostat.[32] The velocities of the atoms were randomly assigned to produce a Maxwell distribution corresponding to 298 K. Each system was simulated for 10 ns with configurations stored every 10 ps for analysis. The equations of motion were integrated using the leapfrog method with a 2 fs time step. Nonbonded interactions were evaluated using a twin range cutoff of 0.8 and 1.4 nm. Interactions within the shorter and longer cutoffs were updated every step and every five steps, respectively. Beyond the 1.4 nm cutoff, a reaction field correction was performed with the same dielectric constant ($\epsilon = 62.0$) employed to parametrize the force field. The bond lengths and H−O−H angle in water were constrained using the SETTLE algorithm;[33] the LINCS[34] algorithm was used to constrain bond lengths in the OGP and cyclodextrin molecules. The analysis of the trajectories was performed using tools of the GROMACS package, the viewers RASMOL[35] 2.7 and VMD[36] 1.8, and programs developed specifically in this work. The number of water molecules inside of the cyclodextrins was calculated using spheres of diameter 0.90, 1.04, and 1.20 nm for α-, β-, and γ-CD, respectively, corresponding to the largest distance between two oxygen atoms linking the glucopyranoside units in the crystal structures of the CDs. At any time in the trajectory, the spheres were centered in the geometrical center of all the oxygen atoms joining the pyranoside rings. The number of hydrogen bonds between cyclodextrin and surfactant molecules was calculated using a cutoff distance between the donor and the acceptor atoms of 0.35 nm and an angle donor−hydrogen−acceptor angle smaller than 30°.

3. Thermodynamic Characterization

3.1. Surface Tension Model for Molecular Assemblies. The systems of interest are ternary mixtures consisting of water and two substances A and B that form molecular assemblies of the general formula A_nB_m. The model developed here is general in the sense that it can deal with systems where both A and B are surface active and systems where only one of them is. If neither A nor B are surface active, surface tension measurements could not be used to characterize the system thermodynamically. As is commonly done when modeling other properties, it is desirable to obtain an expression for the surface tension σ of the ternary mixtures in terms of the surface tensions of the corresponding binary mixtures: A + water and B + water. For this reason, we first present the case of a binary mixture.

To model the experimentally observed change of the surface tension at constant temperature for a binary mixture composed of a surface active substance C and water, it is necessary to relate σ to the concentration of C at the surface. There are several routes to achieve this, the most common being the employment of the Gibbs adsorption equation and the so-called mixing rules. In addition, a relation between the concentration of C in the

bulk liquid and at the liquid−vapor surface is required. To this end, it is necessary to consider the equilibrium established between the processes of adsorption to and desorption from the surface. The rates v for these two processes are given by

$$v_{\text{ads}} = r_1(C_m^s - C^s)C^b \qquad (1)$$

$$v_{\text{des}} = r_2(C_m^b - C^b)C^s \qquad (2)$$

where r_1 and r_2 are constants, C^s and C^b are the concentrations of C at the surface and in the bulk liquid phase expressed in mol L^{-1}, C_m^s is the maximum value of C^s attained when the surface is saturated, and C_m^b is the maximum concentration of C in the bulk liquid; as such, C_m^b can be the solubility limit of C in water or the onset of the formation of some aggregate such as micelles. In eq 1, it is assumed that because the "volume" of the surface phase is much smaller than the bulk volume, C^b is effectively the nominal C concentration, i.e., that used when preparing the binary solution. At equilibrium, $v_{\text{ads}} = v_{\text{des}}$, and the following adsorption isotherm is obtained

$$\theta_C = (\beta C^b)/(C_m^b - C^b + \beta C^b) \qquad (3)$$

with $\beta = r_1/r_2$ and $\theta_C = C^s/C_m^s$. In eq 3, β describes the partition of C between the bulk and the surface. Hence, β measures affinity of C for the surface and gives to θ_C a clear physical meaning as the fraction of the surface covered by the solute. Equation 3 can be used when C is either a surfactant or a substance that is not (or barely) surface active. In the first case, C_m^b is equal to the cmc and hence

$$\theta_C = (\beta C^b)/(\text{cmc} - C^b + \beta C^b) \qquad (4)$$

In eq 4, when the concentration of C in the bulk reaches the cmc $\theta_C = 1$, a limit that other absorption isotherms, e.g., the original Langmuir isotherm,[37] are not able to produce. In the second case, $C^b/C_m^b \ll 1$ and eq 3 simplifies to

$$\theta_C = (\beta^* C^b)/(1 + \beta^* C^b) \qquad (5)$$

with $\beta^* = \beta/C_m^b$. To obtain an expression for the surface tension of the binary mixture σ, the following mixing rule is proposed

$$\sigma = (1 - \theta_C)\sigma_w + \theta_C\sigma_C \qquad (6)$$

where σ_w is the surface tension of pure water and σ_C is the surface tension of the mixture when C has saturated the surface. Combining eqs 3 and 6,

$$\sigma = \sigma_w + \beta C^b(\sigma_C - \sigma_w)/(C_m^b - C^b + \beta C^b) \qquad (7)$$

Because σ_w and C^b are known, eq 7 has three parameters (C_m^b, β, and σ_C) that can be fitted to experimental σ data. However, for some systems, C_m^b and σ_C might be experimentally measured reducing the number of adjustable parameters to only one. Using eq 7, Figure 1a shows the behavior of σ for several values of the σ_C and β parameters. Note that the proposed adsorption isotherm (eq 3) is able to describe the surface saturation region where the Langmuir isotherm fails.

To obtain an expression for the surface tension of ternary mixtures where the two solutes A and B are able to form A_nB_m complexes, it is assumed that eq 3 can be used to represent separately the adsorption of each species

$$\theta_C = (\beta_C C_f^b) / (C_m^b - C_f^b + \beta_C C_f^b) \qquad (8)$$

with C = A or B or $A_n B_m$. In eq 8, all species are considered surface active and subscript f applies only to pure components A and B; i.e., A_f^b and B_f^b are the equilibrium concentrations of free or monomeric A and B in the bulk liquid, respectively. When employing eq 8, it is assumed that the affinities of all species for the surface are mutually independent. This has the advantage that β_A and β_B can be obtained from the corresponding binary mixtures. Using a direct extension of the mixing rule eq 6, the surface tension of the system is

$$\sigma = (1 - \Sigma \theta_C)\sigma_w + \Sigma \theta_C \sigma_C \qquad (9)$$

In eq 8 and 9, A_f^b and B_f^b depend on the number and concentrations of the $A_n B_m$ species formed. For the systems studied in this work, it is assumed that three such species are present. The formation of these molecular complexes is described by the sequential reactions

$$A + B \leftrightarrow AB \qquad AB + A \leftrightarrow A_2B \qquad AB + B \leftrightarrow AB_2$$
$$(10)$$
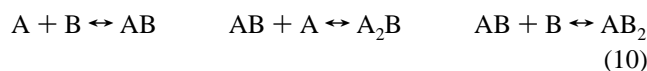
with the apparent equilibrium constants

$$K_{11} = \frac{AB}{A_f^b B_f^b} \qquad K_{21} = \frac{A_2B}{AB\, A_f^b} \qquad K_{12} = \frac{AB_2}{AB\, B_f^b} \qquad (11)$$

In eq 11, AB, A_2B, and AB_2 denote the bulk molar concentrations of the complexes with stoichiometries 1:1, 2:1, and 1:2, respectively. A simple mass balance indicates that

$$A_f^b = A^b - AB - 2A_2B - AB_2 \qquad (12)$$

$$B_f^b = B^b - AB - A_2B - 2AB_2 \qquad (13)$$

with A^b and B^b being the total (nominal) concentrations of A and B in the system. Employing eq 11,

$$A_f^b = A^b - K_{11}A_f^b B_f^b - 2K_{21}K_{11}(A_f^b)^2 B_f^b - K_{12}K_{11}A_f^b(B_f^b)^2 \quad (14)$$

$$B_f^b = B^b - K_{11}A_f^b B_f^b - K_{21}K_{11}(A_f^b)^2 B_f^b - 2K_{12}K_{11}A_f^b(B_f^b)^2 \quad (15)$$

Assuming that the three complexes do not adsorb to the surface, the set of eqs 9, 14, and 15 contain nine parameters, namely A_m^b, B_m^b, β_A, β_B, σ_A, σ_B, K_{11}, K_{21}, and K_{12}, that can be fitted to experimental σ data for the ternary solutions. This large number of parameters can be reduced to only three (K_{11}, K_{21}, and K_{12}) provided the surface tensions for the binaries are also measured. A specifically developed program in C code employing a simulated annealing algorithm,[38] together with the Newton–Raphson algorithm to solve the coupled system of eqs 14 and 15, was employed to fit the parameters. The objective function was

$$S_\sigma = \frac{1}{n} \sum_{i=1}^{n} (\sigma_i^{exp} - \sigma_i^{mod})^2 \qquad (16)$$

where σ_i^{exp} and σ_i^{mod} are the experimental and model evaluated surface tension values and n is the number of experimental values. Other models for the surface tension of systems containing complexes have been reported.[16,39–41] They use the
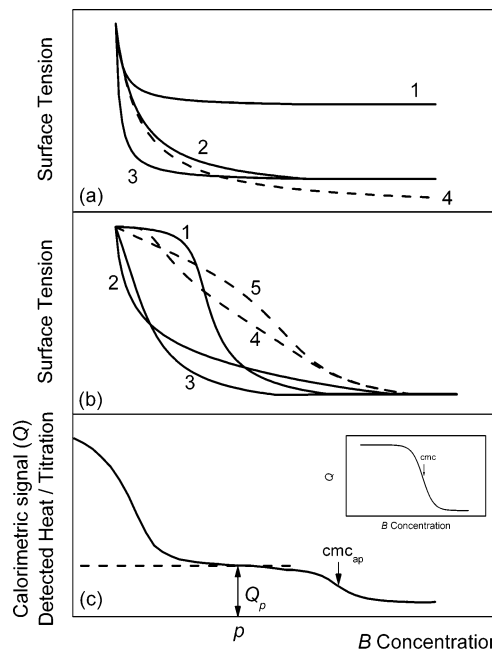

Figure 1. Schematic representation of (a) the surface tension from eq 7 for different values of the σ_B and β parameters. For solid lines 1 to 3, σ_B (1) $>$ σ_B (2) $=$ σ_B (3) and β (1) $=$ β (2) $<$ β (3), all with the same cmc. The dashed line corresponds to the original Langmuir isotherm with the same σ_C and β parameters as in curve 2. (b) Surface tension from eq 9 for different values of the equilibrium constants. For lines 1–3, the dominant species are the 1:1, 1:2, and 2:1 species, respectively. Curves 4 and 5 correspond to mixtures where the three species are simultaneously present. (c) Calorimetric signal from an experiment where a surface active substance B is titrated over a A + water mixture (see text for a detailed description). The inset corresponds to the titration of B over pure water.

original Langmuir isotherm and also differ from the present model in the expression employed to relate σ with the surface concentration. The present model is more flexible because it can be used without the assumption that the complex species do not adsorb to the surface.

Using the model described above, Figure 1b shows schematically the variation of the surface tension with B concentration when $\sigma_A \cong 2\sigma_B$ and $\beta_B \cong 10\beta_A$. Three hypothetical cases are shown, namely those where only one $A_n B_m$ species (1:1, 2:1, or 1:2) is dominant. Also indicated are σ curves for two mixtures where several complexes are simultaneously in equilibrium. Clearly, the model is able to describe the effect that the presence of different species in the bulk liquid has on the surface tension. Hence, fitting the model parameters to experimental σ values would allow one to discern which are the most populated complex stoichiometries.

3.2. Calorimetry. In all calorimetry experiments, an aqueous solution of a surface active substance B at a concentration 10× its cmc was titrated over an A + water mixture, with A being not surface active. Figure 1c shows schematically an example of the variation of the calorimetric signal or detected heat at each titration i, Q_i, with B concentration. Also indicated is the dilution Q_i obtained when the B + water solution was titrated over pure water (inset). Under the experimental conditions, Q_i contains the following contributions: (i) rupture of B micelles, (ii) formation of $A_n B_m$ complexes, (iii) dilution of the free B, i.e., dilution of B molecules not forming part of a micelle, and (iv) dilution of A. Due to the experimental setting of the calorimeter (see Experimental Methods section), contribution iv was automatically subtracted from Q_i. Because the concentration of A in the cell was from 15 to 50× less than the

concentration of B in the syringe, after a number of titrations, practically all A molecules are involved with B molecules forming A_nB_m complexes. In Figure 1c, the concentration of B where this saturation occurs is denoted as p and the corresponding heat value as Q_p. The value of p depends on the stoichiometry of the complexes and on the equilibrium constants for their formation. Contributions i−iii are then present for concentrations of B below p; above p, only contributions i and iii remain. As indicated by Figure 1c, the shape of the curve for concentrations of B greater than p is the same as that for the dilution of B in the absence of A (inset) where only contributions i and iii are present. Hence, $Q_i^{com} = Q_i - Q_p$ is the net calorimetric signal owing to contribution ii, i.e., the heat evolved due to the formation of the A_nB_m complexes. With a further increase in the concentration of B, Figure 1c shows that Q_i decreases toward zero changing in curvature. The inflection point signals the end of contribution i, and hence, the concentration of B where it occurs is the apparent cmc (cmc_{ap}) of B at a given concentration of A. In the absence of A (inset), the inflection point occurs at the cmc of the surface active component B. In this work, a Boltzmann function was fitted to the data to obtain the cmc_{ap} analytically. Both the cmc and the cmc_{ap} can also be evaluated from surface tension as the concentration above which σ remains constant. The cmc and the cmc_{ap} obtained from calorimetry are smaller than those from surface tension, because in the former the formation of micelles in the bulk is detected before the surface becomes saturated.

The analysis of the calorimetric signal in Figure 1c applies to all the A compounds used in this work, the differences among them being the p and Q_p values, as well as the shape of the calorimetric signal in the $(0, p)$ concentration range. In order to obtain the heat involved in the formation of the A_nB_m complexes after j titrations, it is necessary to add Q_i^{com} for all the titrations up to titration j. The accumulated heat (Q_j^{acc}) after j titrations is then

$$Q_j^{acc} = \sum_{i=1}^{j} Q_i^{com} \qquad (17)$$

This experimental Q_j^{acc} can be written in terms of the molar enthalpies of formation ΔH of the complex species considered in this work and their concentrations as

$$Q_j^{acc} = V_j[\Delta H_{11}AB + (\Delta H_{11} + \Delta H_{12})AB_2 + \\ (\Delta H_{11} + \Delta H_{21})A_2B] \quad (18)$$

where V_j is the volume of the mixture in the calorimetric cell, i.e., the original volume placed in the cell plus the volume added after j titrations. In eq 18, the concentrations of the complex species depend on the equilibrium constants for their formation (eqs 14 and 15). Hence, upon fitting to the experimental Q_j^{acc}, there are six adjustable parameters, namely ΔH_{11}, K_{11}, ΔH_{12}, K_{12}, ΔH_{21}, and K_{21}. In this work, we have fixed the equilibrium constants values to those obtained fitting the surface tension data and adjusted only the three enthalpies of formation to the calorimetric data. For this purpose, the fitting protocol described above for the surface tension case was employed, the objective function being

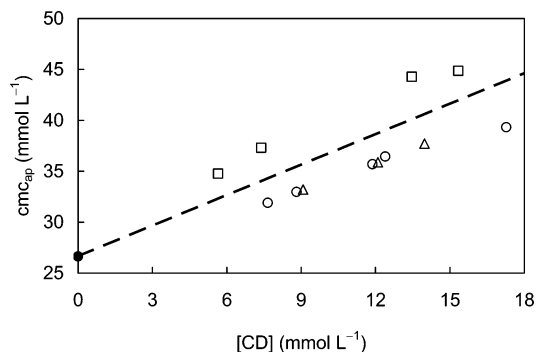$$S_Q = \frac{1}{n} \sum_{i=1}^{n} [Q_i^{acc}(exp) - Q_i^{acc}(mod)]^2 \qquad (19)$$

Figure 2. Apparent cmc of OGP obtained from the calorimetric data against the nominal α- (○), β-, ($\triangle$) and γ-CD (□) concentration. The dashed line of unity slope allows a rough estimate of the species present in solution (see text). The intercept (●) is the cmc (26.6 mM) for OGP obtained as shown in the inset of Figure 1c.

where $Q_i^{acc}(exp)$ and $Q_i^{acc}(mod)$ are the experimental and model evaluated heats and n is the number of experimental values.

4. Results and Discussion

4.1. Screening of Species from Purely Experimental Data. The molecular assemblies studied here are host−guest A_nB_m complexes where A is one of the three native CDs and B the non-ionic surfactant OGP. Figure 2 shows the cmc_{ap} of OGP at different nominal CD concentrations for the three CDs. These cmc_{ap} values were obtained from the calorimetric data as described above (see Figure 1c). The cmc_{ap} is reached when the concentration of free OGP, i.e., not complexed with CD, is equal to its cmc. Hence, cmc_{ap} can be expressed as the sum of the cmc and the concentration of OGP complexed with the CD molecules. As such, it depends on the stoichiometries and equilibrium constants of the species present in the solution. The reference line in Figure 2 represents the ideal case where only 1:1 complexes are present and $K_{11} \rightarrow \infty$. Experimental points above the reference line imply that, in addition to the 1:1 species, other complexes containing more than one OGP molecule are also in solution. From the molecular dimensions and geometry of the molecules involved, the most probable complex is that with a 1:2 stoichiometry. For systems where only 1:1 complexes are present, the cmc_{ap} must be below the reference line; the smaller the K_{11} value the larger the deviation. However, these cmc_{ap} can also be due to the presence of 2:1 complexes, either as the unique species or in equilibrium with the 1:1. Clearly, for A_nB_m inclusion systems where the guest component B is a surfactant, the reference line in Figure 2 separates the region where the most probable species in solution are those with $n < m$ from that where the dominating complexes are those with $n \geq m$. For the present systems, Figure 2 shows that CD-OGP complexes involving α- and β-CD belong to the $n \geq m$ region, and those with γ-CD pertain to the $n < m$ one. Note that this rough screening of species is obtained from purely experimental information. In addition, from geometrical considerations, the most probable stoichiometries in each region can be identified. In what follows, this qualitative knowledge of the system is taken to a quantitative level through the application of a model to experimental surface tension and calorimetric data.

4.2. Host−Guest Equilibrium Constants and Enthalpies of Formation. The experimental liquid−vapor surface tension data at 298.15 K for the binary aqueous solutions of OGP and each of the three CDs are shown in Figure 3. For OGP, the concentration dependence of the surface tension is that of a typical surfactant; i.e., σ decreases sharply at low concentrations
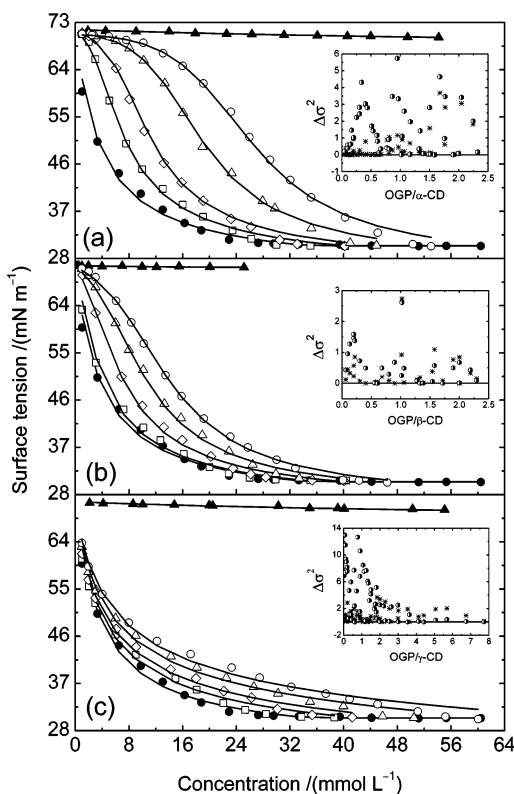
Figure 3. Experimental liquid−vapor surface tension against OGP concentration at 298.15 K for aqueous solutions of OGP with α- (a), β- (b), and γ-CD (c). For α- and γ-CD, the CD nominal concentrations in the ternary mixtures were 5 mM (□), 10 mM (◇), 20 mM (△), and 30 mM (○). For β-CD, the CD nominal concentrations in the ternary mixtures were 1 mM (□), 5 mM (◇), 10 mM (△), and 15 mM (○). Also shown are the surface tensions for the binaries OGP + water (●) and CD + water (▲) (against CD concentration). For each CD, the curves are a simultaneous fit to all the data using the model described in the text, producing the parameters reported in Table 1 (see text for details). The insets show $(\Delta\sigma_i)^2 = (\sigma_i^{exp} - \sigma_i^{mod})^2$ against the ratio of molar concentrations OGP/CD for the global fittings with three species (∗) and considering only the 1:1 stoichiometry (◑).

TABLE 1: Parameters of the Surface Tension and Calorimetry Models[a]

	binary mixtures			
	OGP[b]	α-CD	β-CD	γ-CD
σ	30.4[c]	67.6	71.0	68.0
β^*	282.5	10.7	49.4	14.6
S_σ[d]	0.706	0.003	0.004	0.010

	ternary mixtures		
	α-CD + OGP	β-CD + OGP	γ-CD + OGP
K_{11}	1700	762	7
K_{21}	64	38	46
K_{12}	0	0	509
S_σ[d]	0.49	0.48	0.72
ΔH_{11}	−25.8	−6.4	
ΔH_{21}	−7.3	2.9	
S_Q[e]	1.09×10^{-4}	7.33×10^{-5}	

[a] At 298.15 K, units are mN m^{-1} for σ, L mol^{-1} for β^* and equilibrium constants, and kJ mol^{-1} for enthalpies. [b] The fitted cmc value is 34.8 mM. [c] A value of 26.9 mN m^{-1} is obtained employing the original Langmuir isotherm. [d] Minimum of the objective function, eq 16. [e] Minimum of the objective function, eq 19.

tension, indicates that CD molecules are capable of incorporating themselves into the water network at the surface in such a way that there is no net change of surface energy.

The surface tension data for the ternary mixtures (OGP + CD + water) are also shown in Figure 3. For each cyclodextrin, σ values are plotted as a function of OGP concentration for different fixed CD concentrations. The behavior of σ is different for each CD suggesting the presence of different stoichiometries for the inclusion complexes (see Figure 1). Using the model described in the previous section, for each cyclodextrin, a global fitting, i.e., simultaneously for all CD concentrations, was performed. Because the parameters corresponding to the binary mixtures were obtained independently, only the equilibrium constants for the three species considered were fitted. The only constraint imposed was that all $K > 0$. Several initial sets of K were used, converging always to the same final values. The results are displayed in Figure 3, the parameters being reported in Table 1. The insets in Figure 3 show $(\Delta\sigma_i)^2 = (\sigma_i^{exp} - \sigma_i^{mod})^2$ against the ratio of molar concentrations OGP/CD, demonstrating the excellent performance of the model. Also in these insets $(\Delta\sigma_i)^2$ are shown for the case where only the 1:1 species is considered to be present. Clearly, for α- and γ-CD, an adequate description of the surface tension behavior of these systems demands consideration of species other than the 1:1 complex, particularly at low OGP concentrations. For β-CD, a reasonable description can be obtained assuming the presence of only the 1:1 complex, in agreement with a recent NMR study of the same system.[44] The values of the equilibrium constants in Table 1 indicate that for α- and β-CD the predominant species is 1:1 and to a lesser extent 2:1, disregarding the existence of the 1:2. For γ-CD, the predominant species is the 1:2, the other two species being also present. The null equilibrium constant values in Table 1 are not an artifact of the fitting procedure that in fact finds the global minimum of the objective function (eq 16) with a high probability. It is important to mention that many other fittings with a larger number of parameters (see previous section) were performed. For α- and β-CD, in all these fittings, the standard deviation and the equilibrium constant values did not change significantly with respect to that corresponding to the results in Figure 3. Despite the care taken to ensure a good fitting procedure, for γ-CD, several local minima of the objective function were found, their values being very
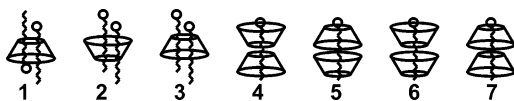
becoming constant at the cmc, where the surface becomes saturated. On the other hand, for the three CDs, σ changes very little with concentration, showing that these cyclodextrins are not surface active. The parameters of the surface tension model described in the previous section were fitted using eq 7 to the data for OGP and each CD, their values being reported in Table 1. The small σ_{OGP} value (as compared to $\sigma = 71.65$ mN m^{-1} for pure water) is indicative of the surface activity of this nonionic surfactant. This value reproduces very well the experimentally observed σ in the saturation region, in contrast to the value obtained if the original Langmuir isotherm is employed (see Table 1). For the three cyclodextrins, the σ_{CD} values are very close to σ for pure water, indicating their poor surface activity. The β^* values for the CDs are much smaller than β^*_{OGP} due to the presence of hydrophilic hydroxyl groups at the rims of their truncated cone shaped geometry, which impose a less hydrophobic character. The β^* value for β-CD is much larger than for α- and γ-CD, in agreement with the fact that β-CD has the lowest solubility in water.[42] The unexpected surface affinity of the CDs signalled by the model has been confirmed by Brewster Angle Microscopy experiments for α-CD,[43] which conclusively demonstrate that cyclodextrins are present in great quantities at the surface. This supports that the present model β^* parameter is a sensitive measure of surface affinity. Being adsorbed at the surface, but only changing slightly the surface

Characterization of Host−Guest Complexes

J. Phys. Chem. B, Vol. 111, No. 17, 2007 **4389**

Figure 4. Schematic representation of the starting conformations for the MD simulations. In the text, these conformations are referred to as **1** (1:2;↓:↓↑), **2** (1:2;↑:↑↑), **3** (1:2;↓:↑↑), **4** (2:1;↑↓:↑), **5** (2:1;↓↑:↑), **6** (2:1;↑↑:↑), and **7** (2:1;↓↓:↑).

close to each other; however, the equilibrium constant values did not change meaningfully. In general, the results for γ-CD indicate that it is not justified to assume[11] that the only inclusion complex formed between γ-CD and guests containing linear hydrocarbon chains (surfactants, alcohols, acids, etc.) is the 1:1 species. Moreover, it is probable that at least one more species might be present in the system, the 2:2 complex being the obvious candidate.

Table 1 reports the enthalpies of formation for the 1:1 and 2:1 complexes obtained through a global fitting to the experimental accumulated heats, i.e., a simultaneous fit for all CD concentrations. For these determinations, the equilibrium constants in eq 18 were fixed to the values obtained by fitting to the surface tension data. The drastic change for ΔH_{11} in going from α- to β-CD has been reported previously for guests containing linear hydrocarbon chains.[11] For γ-CD, the accumulated heats are very small. The largest values are on the order of 0.05 J and vary little with the concentration ratio OGP/ CD. This presents a difficulty for fitting the three enthalpies corresponding to the 1:1, 2:1, and 1:2 species, the presence of which are indicated by the surface tension measurements. The net result is that upon minimization of the objective function many local minima appear and the uncertainty in the enthalpy is too large for the values to be considered reliable.

4.3. Structure and Dynamics of the Host−Guest Complexes. For each of the three cyclodextrins with OGP, MD simulations were performed using as starting conformations the seven structures depicted in Figure 4. Employing the methodology and conditions detailed in the Experimental Methods Section, the duration of each of the 21 simulations was 10 ns. This time scale was sufficient to observe spontaneous dissociation of the unstable structures and in one case the spontaneous reformation of a complex. Such events within the same trajectory and without the application of restraints are rarely found in atomistic MD simulations.[45] The conformations found to be stable in the MD simulations are in agreement with those inferred from the surface tension data. Analysis of the MD trajectories suggest that hydrophobic interactions between the CD host and the OGP guest are primarily responsible for the formation and stability of the inclusion complexes. Another relevant and general result is that in the stable inclusion complexes the CD molecules lose their original truncated cone shape and adopt a cylindrical geometry. For clarity, the presentation and discussion of the most significant results of the MD simulations are given separately for each CD. The initial and final conformations for the 21 trajectories are given in the Supporting Information.

4.3.1. Simulations of α-CD-OGP complexes. For the starting conformations **1** (1:2;↓:↓↑) and **2** (1:2;↑:↑↑) in Figure 4, one OGP molecule left the CD cavity in few nanoseconds, leading to stable 1:1 complexes. For structure **3** (1:2;↓:↑↑), both OGP molecules were lost from the CD cavity. These findings support the conclusions from the surface tension and calorimetric data that the 1:2 species is not stable. Starting from two of the 2:1 structures, **4** (2:1;↑↓:↑) and **7** (2:1;↓↓:↑), one CD was lost with again a 1:1 complex being formed. In the case of structure **6** (2:1;↑↑:↑), the aggregate disassociated, but for conformation **5**
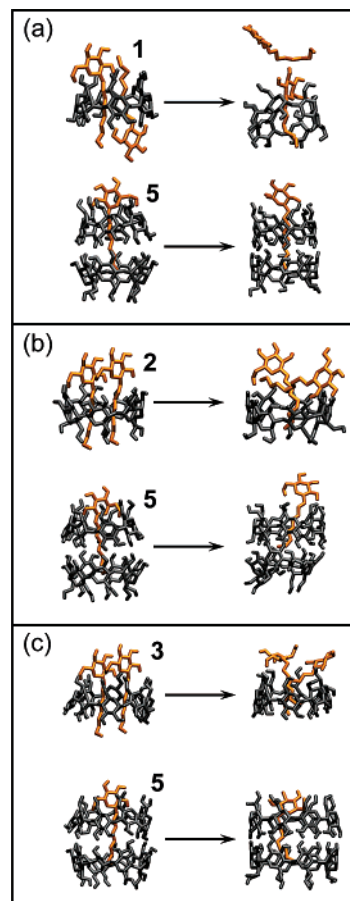

Figure 5. Initial and final conformations after 10 ns of MD simulations for some inclusion complexes of α- (a), β- (b), and γ-CD (c) with OGP. The numbers in the upper right corner of the initial structures correspond to the labels used in Figure 4. For clarity, water molecules are not displayed.

(2:1;↓↑:↑), the original 2:1 stoichiometry was kept. This is consistent with the nonzero equilibrium constant for this species in Table 1. Starting from **1** (1:2;↓:↓↑), the OGP molecule that left the complex was that initially oriented with its head close to the wide size of the truncated cone shape of the α-CD. As a result, in the final 1:1 complex, the OGP head is close to the side of the CD containing the secondary hydroxyl groups (↓:↑). In contrast, starting from **2** (1:2;↑:↑↑), the final 1:1 complex has the OGP head close to the side of the CD containing the primary hydroxyl groups (↓:↓). Hence, it appears that both orientations of the OGP molecule are feasible, and from the current MD simulations, it is not possible to determine which orientation is the more stable.

Figure 5a shows the final structures obtained from the initial conformations **1** (1:2;↓:↓↑) and **5** (2:1;↓↑:↑). In order to explore the dynamic behavior of these systems, the distances between the centers of geometry of each molecule and the root-mean-square positional deviation of the aggregate with respect to the initial structure were calculated as a function of time. Figure 6a,b shows these quantities for the trajectories of the two examples shown in Figure 5a. For the starting structure **1** (1:2;↓:↓↑), it can be seen from Figure 6a that the distance between the CD and one of the OGP molecules, as well as the distance between the two OGP molecules, have a sharp peak at 2 ns, corresponding to the point at which one of the surfactant molecules leaves the CD cavity. For a while, this OGP molecule interacts closely with the remaining 1:1 complex but does not again penetrate the CD cavity. Finally, between 4 and 5 ns this
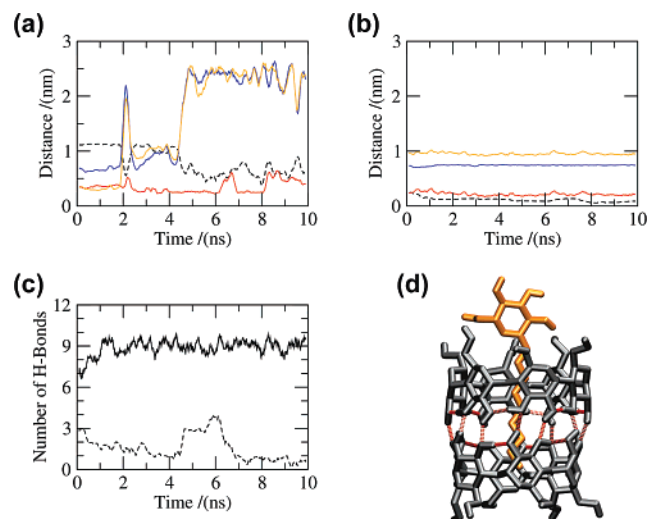
Figure 6. Selected intermolecular distances for the two trajectories indicated in Figure 5a. In part a, the starting conformation was structure **1** (1:2;↓:↓↑), the indicated distances being OGP−OGP (blue) and α-CD-OGP for each of the surfactant molecules (red and yellow). In part b, the starting conformation was structure **5** (2:1;↓↑:↑), the indicated distances being α-CD-α-CD (blue) and α-CD-OGP for each of the cyclodextrin molecules (red and yellow). The dashed lines in parts a and b are the rmsd of the aggregates. For the trajectory starting from conformation **5** (2:1;↓↑:↑), the number of intermolecular α-CD-α-CD (solid line) and α-CD-OGP (dashed line) H-bonds are shown in part c. The inter- and intramolecular H-bonds involving the two α-CD molecules in the final structure of the 2:1 complex are shown in part d; for clarity, water molecules are not displayed.

OGP molecule separates completely from the remaining 1:1 complex. In contrast, Figure 6b shows that for structure **5** (2:1;↓↑:↑) all the intermolecular distances remain approximately constant throughout the simulation. The number of water molecules inside the cyclodextrin was also calculated as a function of time. For free α-CD, the number of water molecules inside the cavity fluctuates between four and six (MD results not shown). The analysis of the seven trajectories indicates that the inclusion of an OGP molecule partially or in some cases totally displaces these water molecules. All water molecules are displaced when the OGP molecule occupies the whole cavity. This is the case for the final conformation starting from **1** (1:2;↓:↓↑) and for the CD that is close to the polar head of OGP starting from **5** (2:1;↓↑:↑) in Figure 5a. Because the CD further away from the head of the OGP molecule contains only a fraction of its hydrocarbon tail, the number of water molecules inside this cavity varies between two and three.

The final conformation in the simulation initiated from structure **5** (2:1;↓↑:↑) and shown in Figure 5a deserves further discussion. In this structure, the two CD molecules face each other through the wide side of the cone. During the trajectory, not only is this initial structure kept but the packing is increased. As indicated in Figure 6c,d, this tight packing is due to the presence of an average of nine intermolecular H-bonds formed between the two CD molecules, intramolecular H-bonds being also present. Figure 6d also indicates that in this H-bonded CD dimer the original truncated cone shape of each CD switches to a cylindrical geometry. Because each α-CD molecule contributes with 12 hydroxyl groups to the interface region, the maximum possible number of H-bonds between the two CDs is almost reached at any time. Note that this packing arrangement is unique to this structure and none of the other 2:1 complexes were found to be stable. Recent scanning tunneling microscopy studies of α-CD necklaces threaded on to poly-
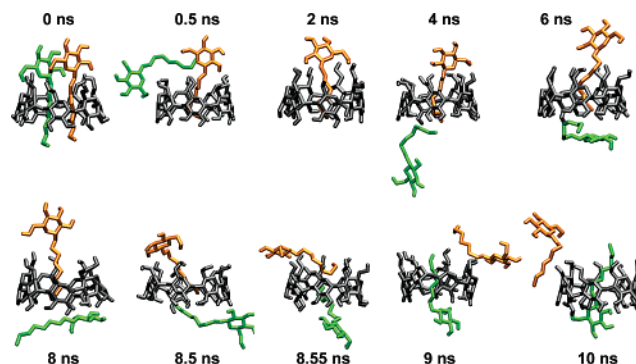

Figure 7. Snapshots at the indicated times for the trajectory of the 2:1 complex with β-CD starting from the structure **3** (1:2;↓:↑↑) in Figure 4. At 2 ns, one OGP molecule in the simulation box is far away from the 1:1 complex and it is not shown to keep the same scale. For clarity, water molecules are not displayed. A movie showing the 10 ns MD simulation is available (cf. Supporting Information).

(ethylene glycol) indicated that the head−head and tail−tail conformations (structures **5** (2:1;↓↑:↑) and **4** (2:1;↑↓:↑) in Figure 4, respectively) account for 80% of the CD dimer population.[7] Our results suggest that the main contribution to the stability of necklaces may arise from the head−head dimers. Performing MD simulations of α-CD necklaces with long guest molecules is a clear avenue for future work. As indicated in Figure 6c, a small and fluctuating number of H-bonds are formed between the hydroxyl groups in the OGP head and the hydroxyl groups in the CD molecule. A similar behavior was also found in the final conformations emerging from the initial structures **4** (2:1;↑↓:↑), **6** (2:1;↑↑:↑), and **7** (2:1;↓↓:↑). These H-bonds are not critical for the stability of the complexes that is dominated by the hydrophobic interactions between the CD cavity and the OGP hydrocarbon chain.

4.3.2. Simulations of β-CD-OGP Complexes. In general, the results for β-CD are similar to those just described for α-CD. For the starting conformations **1** (1:2;↓:↓↑) to **3** (1:2;↓:↑↑) in Figure 4, the final structure was a 1:1 complex; i.e., as in the case of α-CD with initial conformations **1** (1:2;↓:↓↑) and **2** (1:2;↑:↑↑), only one OGP molecule remains in the CD cavity after a few nanoseconds. The presence of a stable 1:1 species and the absence of 1:2 complexes again support the conclusions reached from the surface tension and calorimetric data. Of particular interest is that the 10 ns trajectory starting from conformation **3** (1:2;↓:↑↑) in Figure 4 showed the spontaneous exchange of the guest molecule. This is illustrated in Figure 7, which shows a series of snapshots of the trajectory detailing the sequence of events during the exchange. First, the spontaneous release of one OGP molecule from the 1:2 complexes is observed leading to a 1:1 species. Second, the free OGP returns to the vicinity of the CD cavity. Third, there is competition between the two OGP molecules to occupy the cavity, and finally, the OGP molecule within the cavity is displaced by the other one, producing another 1:1 complex. A movie showing this rare exchange event is available (cf. Supporting Information). In the simulations starting from structures **6** (2:1;↑↑:↑) and **7** (2:1;↓↓:↑), one of the CD molecules is lost from the initial complex, leading to a 1:1 species. In the simulations starting from structure **4** (2:1;↑↓:↑), the three molecules remain together but the final conformation is more an unstructured aggregate rather than an inclusion complex. For conformation **5** (2:1;↓↑:↑), the original 2:1 stoichiometry was again conserved, in agreement with the nonzero equilibrium constant for this species in Table 1. Figure 5b shows the final structures obtained from the initial conformations **2** (1:2;↑:↑↑) and **5** (2:1;↓↑:↑). The structure obtained starting from **2**

Characterization of Host−Guest Complexes

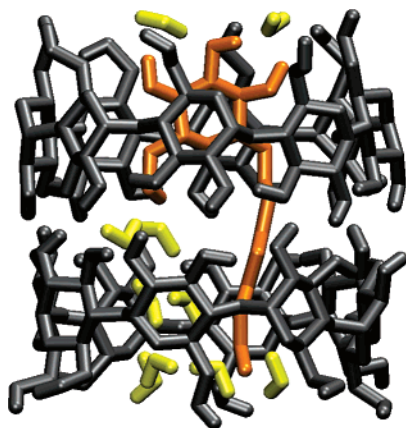*J. Phys. Chem. B, Vol. 111, No. 17, 2007* **4391**

Figure 8. Water molecules (yellow) within the CD cavities for the 2:1 inclusion complex formed by γ-CD and OGP. The starting conformation was **5** (2:1;↓↑:↑) in Figure 4, and the displayed structure is a representative one from the trajectory. For clarity, all other water molecules are not shown.

(1:2;↑:↑↑) is not a typical 1:2 inclusion complex because the hydrophobic tail of one of the OGP molecules is not inside of the CD cavity. However, this structure remained stable for almost the complete simulation, suggesting that, in addition to the classical inclusion complexes, such a kind of species might also be present in cyclodextrin−surfactant mixtures. Note that the final structure obtained starting from conformation from **5** (2:1;↓↑:↑) and illustrated in Figure 5b is much less compact than the conformation seen for α-CD in Figure 5a. Even though there are more hydroxyl groups available to form H-bonds between the two CD molecules in β- than in α-CD, the average number of intramolecular H-bonds is only six for β-CD contrasting with nine in the case of α-CD. For free β-CD, the number of water molecules inside the cavity is approximately eight (MD results not shown). In contrast to the case of α-CD, the OGP shares the CD cavity with an average of two water molecules in the 1:1 complex. This is due to the cavity in β-CD being larger than in α-CD. For the 2:1 complex shown in Figure 5b resulting from structure **5** (2:1;↓↑:↑), three to four water molecules remain in the cavity of the CD that is closer to the end of the OGP tail.

4.3.3. Simulations of γ-CD-OGP Complexes. As shown in Figure 5c and in contrast to the results for α- and β-CD, for γ-CD, the species with stoichiometry 1:2, resulting from the initial conformation **3** (1:2;↓:↑↑), is stable at least on the time scales of the simulations. From structures **1** (1:2;↓:↓↑) and **2** (1:2;↑:↑↑), a 1:1 complex and an unstructured aggregate were obtained, respectively. The initial conformations **6** (2:1;↑↑:↑) and **7** (2:1;↓↓:↑) also resulted in a 1:1 complexes; **4** (2:1;↓↑:↑) and **5** (2:1;↓↑:↑) maintained their original 2:1 stoichiometry. These results support the coexistence in equilibrium of the three species indicated by the surface tension and calorimetric data analysis. The 2:1 complex in Figure 5c is quite similar to the corresponding structure for α-CD shown in Figure 5a. Both structures share two characteristics, namely many intramolecular H-bonds between the two CD molecules (12 out of a maximum possible of 16 for γ-CD), and that they undergo a switch from a cone-shape geometry to a cylindrical one. They do differ, however, in the number of water molecules sharing the CD cavity with the OGP molecule. The snapshot in Figure 8 shows that water molecules are present in both cavities, a similar distribution being observed throughout the whole 10 ns trajectory. The large cavity of γ-CD is clearly responsible for the presence of such a substantial amount of water molecules that, in fact, can rise to sixteen for each free γ-CD in solution (MD results not shown).

5. Conclusions

By using a combination of surface tension, calorimetry, and molecular dynamics simulations, we have been able to characterize in detail host−guest complexes formed between α-, β-, and γ-cyclodextrin and the non-ionic carbohydrate surfactant octyl-β-D-glucopyranoside. It has been shown that for α- and β-CD the predominant species is the 1:1 complex, that the 1:2 complex is absent, and that significant quantities of the 2:1 complex are present. In the case of γ-CD, the 1:2 species dominates, with the 1:1 and 2:1 complexes being also present. These findings clearly demonstrate that the often used assumption that only a 1:1 species needs to be considered is inappropriate.

The work also demonstrated that, using only calorimetric data, a rough screening of the most probable complex stoichiometries for any host−guest system can be obtained in a model free form. Using a model that includes a newly proposed adsorption isotherm, we analyzed the surface tension data, allowing the evaluation of the equilibrium constants for several stoichiometries. Finally, MD simulations have been used to afford independent support for the stoichiometries determined by the experimental data, also providing valuable information regarding the structures and interactions involved in the host−guest complexes. Overall, the work shows the power with which complimentary experimental and modeling techniques can be combined to better understand the nature of molecular assemblies in solution.

Supporting Information Available: Initial and final conformations for the 21 MD trajectories, their coordinates being available upon request to the authors; a movie showing spontaneous dissociation−formation for the host−guest system composed by one β-CD and two OGP molecules. This material is available free of charge via the Internet at http://pubs.acs.org.

References and Notes

(1) Badjic, J. D.; Balzani, V.; Credi, A.; Silvi, S.; Stoddart, J. F. *Science* **2004**, *303* (5665), 1845−1849.

(2) Balzani, V.; Credi, A.; Raymo, F. M.; Stoddart, J. F. *Angew. Chem., Int. Ed.* **2000**, *39* (19), 3349−3391.

(3) Nguyen, T. D.; Tseng, H. R.; Celestre, P. C.; Flood, A. H.; Liu, Y.; Stoddart, J. F.; Zink, J. I. *Proc. Natl. Acad. Sci. U.S.A.* **2005**, *102*, (29) 10029−10034.

(4) Harada, A. *Acc. Chem. Res.* **2001**, *34* (6), 456−464.

(5) Benenson, Y.; Gil, B.; Ben-Dor, U.; Adar, R.; Shapiro, E. *Nature* **2004**, *429* (6990), 423−429.

(6) Cacialli, F.; Wilson, J. S.; Michels, J. J.; Daniel, C.; Silva, C.; Friend, R. H.; Severin, N.; Samori, P.; Rabe, J. P.; O'Connell, M. J.; Taylor, P. N.; Anderson, H. L. *Nat. Mater.* **2002**, *1* (3), 160−164.

(7) Miyake, K.; Yasuda, S.; Harada, A.; Sumaoka, J.; Komiyama, M.; Shigekawa, H. *J. Am. Chem. Soc.* **2003**, *125*, (17), 5080−5085.

(8) Sousa, S. F.; Fernandes, P. A.; Ramos, M. J. *Proteins: Struct., Funct., Bioinformatics* **2006**, *65* (1), 15−26.

(9) Verkhivker, G. M.; Bouzida, D.; Gehlhaar, D. K.; Rejto, P. A.; Freer, S. T.; Rose, P. W. *Curr. Opin. Struct. Biol.* **2002**, *12* (2), 197−203.

(10) Minton, A. P. *J. Biol. Chem.* **2001**, *276* (14), 10577−10580.

(11) Rekharsky, M. V.; Inoue, Y. *Chem. Rev.* **1998**, *98* (5), 1875−1917.

(12) Janos, P. *J. Chromatogr., A* **2004**, *1037* (1−2), 15−28.

4392 *J. Phys. Chem. B, Vol. 111, No. 17, 2007*

Piñeiro et al.

(13) Tanaka, Y.; Terabe, S. *J. Chromatogr., B: Biomed. Appl.* **2002**, *768* (1), 81−92.

(14) Guo, W.; Fung, B. M.; Christian, S. D. *Langmuir* **1992**, *8* (2), 446−451.

(15) Winzor, D. J. *J. Chromatogr., A* **2004**, *1037* (1−2), 351−367.

(16) Angelova, A.; Ringard-Lefebvre, C.; Baszkin, A. *J. Colloid Interface Sci.* **1999**, *212* (2), 280−285.

(17) Baumy, P.; Morin, P.; Dreux, M.; Viaud, M. C.; Boye, S.; Guillaumet, G. *J. Chromatogr., A* **1995**, *707* (2), 311−326.

(18) Rekharsky, M. V.; Inoue, Y. *J. Am. Chem. Soc.* **2002**, *124* (5), 813−826.

(19) Wren, S. A. C.; Rowe, R. C. *J. Chromatogr.* **1992**, *603* (1−2), 235−241.

(20) Marrink, S. J.; Tieleman, D. P.; Mark, A. E. *J. Phys. Chem. B* **2000**, *104* (51), 12165−12173.

(21) de Vries, A. H.; Mark, A. E.; Marrink, S. J. *J. Am. Chem. Soc.* **2004**, *126* (14), 4488−4489.

(22) Daura, X.; Jaun, B.; Seebach, D.; van Gunsteren, W. F.; Mark, A. E. *J. Mol. Biol.* **1998**, *280* (5), 925−932.

(23) Daura, X.; van Gunsteren, W. F.; Mark, A. E. *Proteins: Struct., Funct., Genet.* **1999**, *34* (3), 269−280.

(24) Piñeiro, Á.; Villa, A.; Vagt, T.; Koksch, B.; Mark, A. E. *Biophys. J.* **2005**, *89* (6), 3701−3713.

(25) Piñeiro, Á.; Brocos, P.; Amigo, A.; Pintos, M.; Bravo, R. *J. Chem. Thermodyn.* **1999**, *31* (7), 931−942.

(26) Berendsen, H. J. C.; van der Spoel, D.; van Drunen, R. *Comput. Phys. Comm.* **1995**, *91* (1−3), 43−56.

(27) Lindahl, E.; Hess, B.; van der Spoel, D. *J. Mol. Modeling* **2001**, *7* (8), 306−317.

(28) http://www.gromacs.org.

(29) Berendsen, H. J. C.; Postma, J. P. M.; van Gunsteren, W. F.; Hermans, J., *Interaction models for water in relation to protein hydration*; Reidel D. Publishing Company: Dordrecht, 1981; p; 331−342.

(30) Schuler, L. D.; van Gunsteren, W. F. *Mol. Simul.* **2000**, *25* (5), 301−319.

(31) Oostenbrink, C.; Villa, A.; Mark, A. E.; van Gunsteren, W. F. *J. Comput. Chem.* **2004**, *25* (13), 1656−1676.

(32) Berendsen, H. J. C.; Postma, J. P. M.; van Gunsteren, W. F.; DiNola, A.; Haak, J. R. *J. Chem. Phys.* **1984**, *81*, 3684−3690.

(33) Miyamoto, S.; Kollman, P. A. *J. Comput. Chem.* **1992**, *13*, 952−962.

(34) Hess, B.; Bekker, H.; Berendsen, H. J. C.; Fraaije, J. *J. Comput. Chem.* **1997**, *18* (12), 1463−1472.

(35) Sayle, R. A.; Milnerwhite, E. J. *Trends Biochem. Sci.* **1995**, *20* (9), 374−376.

(36) Humphrey, W.; Dalke, A.; Schulten, K. *J. Mol. Graphics* **1996**, *14* (1), 33−38.

(37) Langmuir, I. *J. Am. Chem. Soc.* **1918**, *40*, 1361−1402.

(38) Press, W. H.; Teukolsky, S. A.; Vetterling, W. T.; Flannery, B. P., *Numerical Recipes in C++. The Art of Scientific Computing*, 2nd ed.; Cambridge University Press: Cambridge, 2002.

(39) Dharmawardana, U. R.; Christian, S. D., Tucker, E. E.; Taylor, R. W.; Scamehorn, J. F. *Langmuir* **1993**, *9*, 2258−2263.

(40) Funasaki, N.; Yodo, H.; Hada, S.; Neya, S. *Bull. Chem. Soc. Jpn.* **1992**, *65*, 1323−1330.

(41) Funasaki, N.; Ohigashi, M.; Hada, S.; Neya, S. *Langmuir* **2000**, *16* (2), 383−388.

(42) Saenger, W. R.; Jacob, J.; Gessler, K.; Steiner, T.; Hoffmann, D.; Sanbe, H.; Koizumi, K.; Smith, S. M.; Takaha, T. *Chem. Rev.* **1998**, *98* (5), 1787−1802.

(43) This laboratory, unpublished work.

(44) Reinsborough, V. C.; Stephenson, V. C. *Can. J. Chem.* **2004**, *82* (1), 45−49.

(45) Varady, J.; Wu, X. W.; Wang, S. M. *J. Phys. Chem. B* **2002**, *106* (18), 4863−4872.